International Scholarly Research Network
ISRN Meteorology
Volume 2012, Article ID 529401, 16 pages
doi:10.5402/2012/529401

Research Article

Implementation and Validation of Dynamical Downscaling in a Microscale Simulation of a Lake Michigan Land Breeze

Gijs de Boer,[1,2,3] Gregory J. Tripoli,[4] and Edwin W. Eloranta[4]

[1] *Cooperative Institute for Research in Environmental Sciences, The University of Colorado-Boulder, Boulder, CO 80305, USA*
[2] *Physical Sciences Division, NOAA Earth System Research Laboratory, Boulder, CO 80305, USA*
[3] *Earth Sciences Division, Lawrence Berkeley National Laboratory, Berkeley, CA 94720, USA*
[4] *Department of Atmospheric and Oceanic Sciences, The University of Wisconsin-Madison, Madison, WI 53706, USA*

Correspondence should be addressed to Gijs de Boer, gijs.deboer@colorado.edu

Received 1 May 2012; Accepted 25 May 2012

Academic Editors: N. A. Mazzeo, U. Rizza, K. K. Szeto, and J. Xiao

A nested numerical simulation of a land breeze observed over the western Lake Michigan shoreline was completed using the University of Wisconsin Nonhydrostatic Modeling System. This simulation was compared against observations obtained using a variety of instrumentation, most notably a scanning lidar system. The simulated land breeze is shown to closely represent the observations. Most notably, the influence of synoptic scale evolution on the strength and extent of the land breeze is illustrated to be a critical factor in accurately simulating the lifetime of the land breeze. Additionally, model resolution is shown to impact the ability of the simulation to accurately portray the fine scale features of the land breeze circulation, including the depth of the land breeze front and interactions between the land breeze and prevailing synoptic scale flow.

1. Introduction

Micro-α and smaller boundary layer phenomena are often those observed most directly by the general population. Numerical simulation of these types of phenomena has been accomplished mainly through use of Large-Eddy Simulation (LES) (e.g., [1, 2]). LES experiments typically involve high-resolution (10s of meters or higher) simulation, using highly idealized cases with well-established boundary conditions. Although conditions representative of the large- (meso-α and larger, here defined as the scale of fronts and hurricanes [3]) scale weather pattern can be applied at simulation initialization, LES typically does not account for evolution of that scale. Therefore, these simulations usually lack the evolving influence of meso- and synoptic-scale structures.

Use of LES is justified in part by the idea that local processes dominate at small scales, and that statistics of the local boundary layer state are a sufficiently accurate representation of the general atmosphere. Often, however, evolution of the large-scale atmospheric state leads to significant modification of local-scale flow. Typically this occurs in one of two ways: (1) large-scale flow alters a separate circulation initiated through local instability or (2) localized variation in surface properties directly transform the large-scale flow. Examples of the first type of interaction are sea or land breezes. The circulation is initiated by a local-scale gradient in surface temperature, yet the large-scale flow still largely controls the extent and evolution of the final circulation [4]. Examples of the second kind of interaction would be funneling of wind through city corridors by obstacles such as tall buildings, or alteration of large-scale wind by topographical or shoreline features. Without a large-scale pressure gradient, there would be no wind to funnel down specific city streets, and shoreline variation can lead to organization of boundary layer roll structures under correct conditions [5]. Because of these interactions, simulation of the atmospheric boundary layer is ultimately connected to accurate reproduction of processes at meso-α and larger scales and, as importantly, their evolution.

An alternative method for simulation of these highly localized events is the use of dynamical downscaling. This is normally accomplished via nesting of higher resolution grids within lower resolution model domains, and has been utilized to study localized processes within a simulation of a

large-scale scenario where large-scale evolution is crucial to the lifecycle of the studied phenomenon. Examples include regional climate simulations (e.g., [6, 7]), studies of tropical cyclones (e.g., [8, 9]), others) and studies of continental convective systems (e.g., [10, 11]); others).

Local-scale circulations can have significant impacts upon pollution dispersion along industrial coastlines [12, 13]. Additionally, these circulations can enhance snowfall along the Great Lakes, with winter land breezes creating a convergence zone offshore between prevailing flow and the circulation [14–18]. Early studies of land breeze dynamics (e.g., [19–21]) illustrate that the main factors determining land breeze formation were shown to include strength and direction of the gradient wind [22–24] and strength of the land-sea (or lake) temperature contrast, resolved along with topography.

In this study we evaluate a dynamically downscaled simulation of a land breeze circulation observed on December 21, 1997 with the University of Wisconsin Volume-Imaging Lidar (UW-VIL). The VIL was positioned at Sheboygan Point, WI (Figure 1) during the Lake-Induced Convection Experiments (Lake-ICE, [25]). Details of atmospheric conditions of the date and the land breeze itself will be discussed in Section 3. There are several data sources from the date, including temperature and wind observations from the National Data Buoy Center (NDBC) site at Sheboygan Point, approximately 1 km from the VIL position. VIL observations are used as the primary validation tool for the simulation solution, since traditional observing networks do not provide adequate detail at these small scales in multiple dimensions.

In addition to analysis of the ability of a dynamically downscaled simulation to accurately represent a land-breeze flow, the effect of resolution on simulation results is evaluated. Previous efforts [26, 27] demonstrate that increased resolution deepens our insight into structural features at small scales. These improvements, however, were typically made in replication of statistics of a flow rather than in accurate representation of the physical structure of the flow itself. In this study, it is believed that central factors affecting land breeze intensity, depth, and horizontal extent are those from meso-α scale features such as strength and direction of the large-scale flow and position of mesoscale frontal systems, along with highly resolved and highly predictable land surface features. Microscale eddies are expected to only influence the small-scale variance of the flow. Therefore, it is believed that predictability of the micro-α scale will take on that of larger scales.

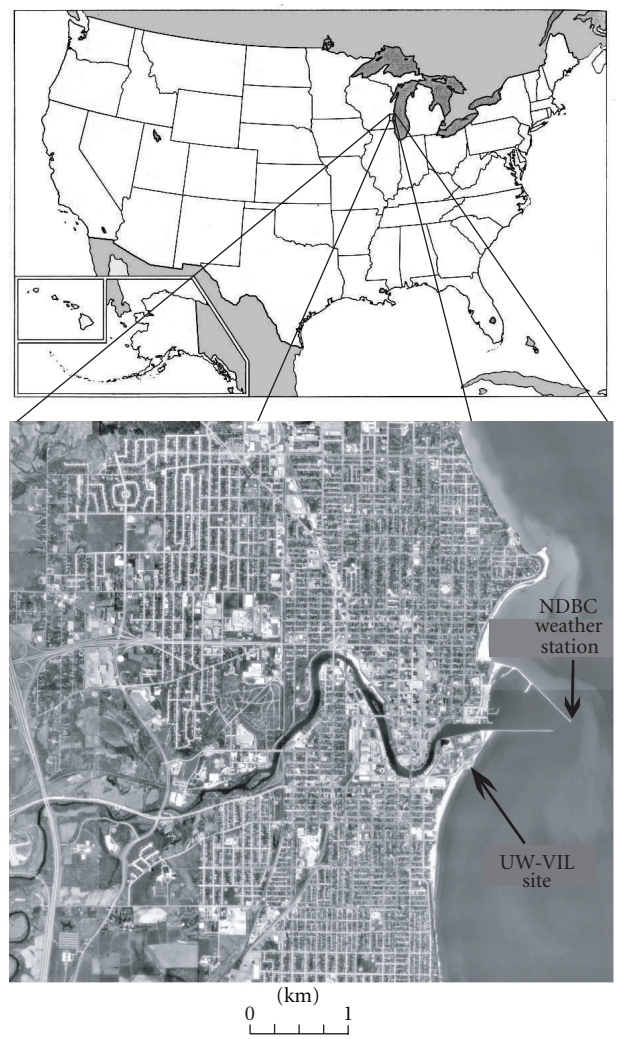

Figure 1: A map showing the location of the Volume Imaging Lidar during the Lake-ICE experiments, as well as the NDBC Observation station.

2. The University of Wisconsin Nonhydrostatic Modeling System (UW-NMS)

The University of Wisconsin Nonhydrostatic Modeling System (UW-NMS, [28]) is designed to properly simulate a wide range of scales and the interactions between them. Implementation of the grid-nesting capability of the UW-NMS accomplishes simultaneous simulation of both meso-α and larger and micro-α (200 m–2 km) and smaller scales. The nesting technique interpolates a large-scale deterministic forecast produced from observed initial conditions to higher resolutions in a specific part of the domain. This higher resolution nest is then integrated forward in time with lateral boundary conditions that evolve as they interact with the parent grid. Here, we evaluate the ability of a dynamically downscaled simulation to correctly simulate the structure and evolution of events at the fine scale (micro-α and below), when given a meso-α or lower resolution initial state together with high resolution topography and surface conditions.

The UW-NMS is a quasicompressible, nonhydrostatic model utilizing a 1.5-order TKE turbulence closure scheme. It has two features that give it an advantage over other models in execution of dynamically downscaled simulations. The first of these is a multiple two-way grid nesting capability. This allows for investigation into interaction between processes at the mesoscale and larger and those occurring at the micro scale. A second advantageous feature of the UW-NMS is that it utilizes a variably stepped topography scheme. Since it is being hypothesized that small-scale structures in this case are due in large part to resolution of topographical

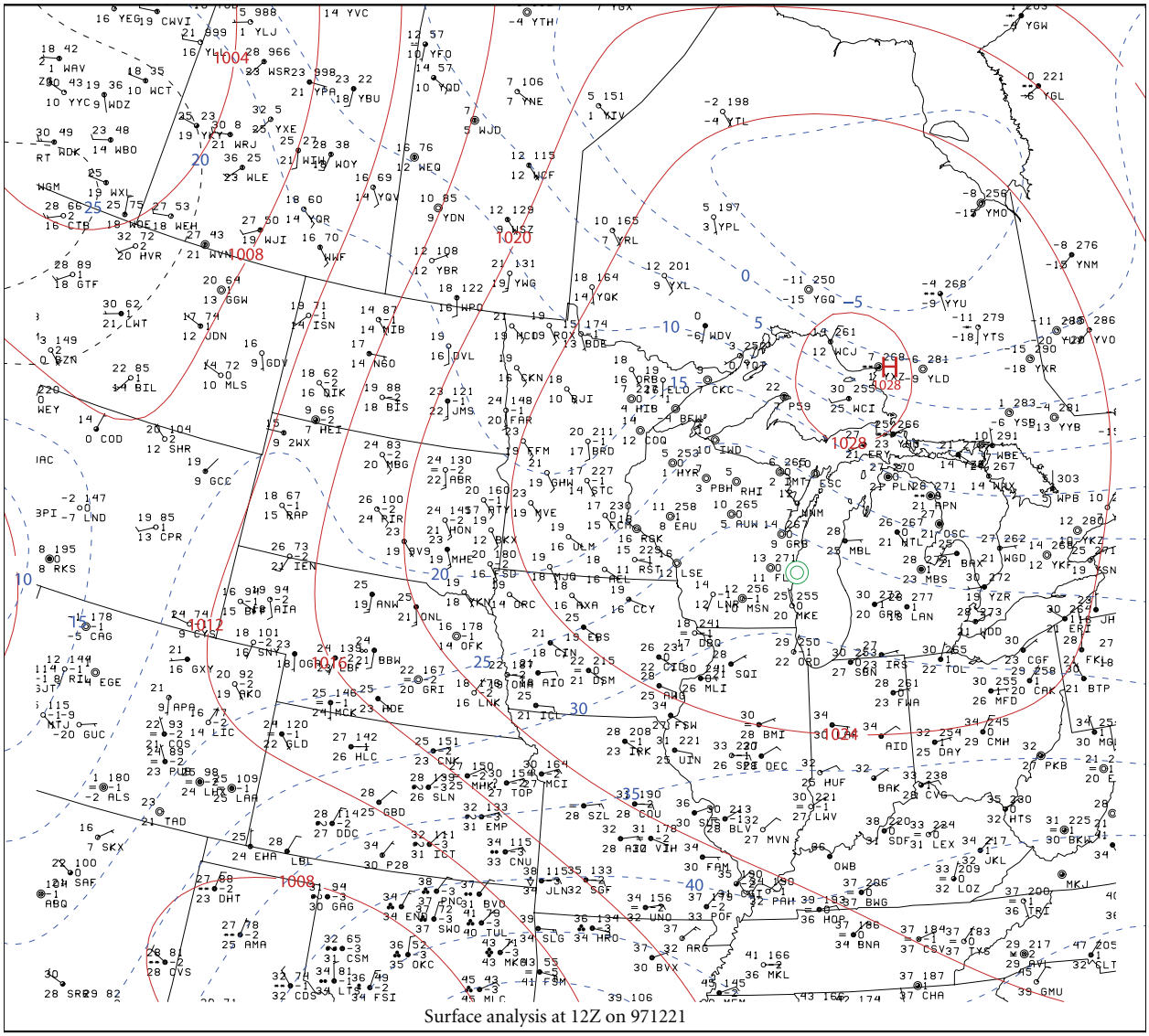

Figure 2: Surface observations at 12:00 GMT on December 21, 1997. Included are contours of pressure (red) and temperature (blue) as well as the location of Sheboygan, Wisconsin (green circle).

and land surface conditions, being able to reproduce them with increased accuracy is vital. Unlike traditional terrain-following or simple stepped topography schemes, variably stepped topography allows for the accurate representation of both very steep and gradual topographical differences.

3. The University of Wisconsin Volume-Imaging Lidar (UW-VIL)

The UW-VIL is an elastic backscatter lidar designed for four-dimensional data collection of the atmospheric boundary layer. The system transmitter operates at 1064 nm, with an average power of 40 watts, and a 100 Hz repetition rate. The receiver utilizes a 0.5 m telescope set up in a Cassegrain configuration, with a 1 nm optical bandwidth. This allows for 15 m range resolution and a maximum angular scan rate of around 20 degrees per second. The combination of a powerful laser, large telescope, and high quantum efficiency detector allows for detection of aerosol structures up to a range of 30 km in a clear atmosphere.

Since molecular scattering is relatively small at 1064 nm, the backscatter is largely dependent upon aerosol distribution in the atmosphere. Because of this sensitivity, differing aerosol concentrations—as are often found inside convective boundary layer structures—are easily detected.

For boundary layer applications, three main scan strategies are employed. The first involves keeping the azimuth angle constant while scanning between elevation angles; this is known as a range-height indicator (RHI). The second is a similar technique, but after each RHI is completed, the azimuth changes, creating an RHI volume scan. The third scanning strategy utilized is a plane parallel indicator scan

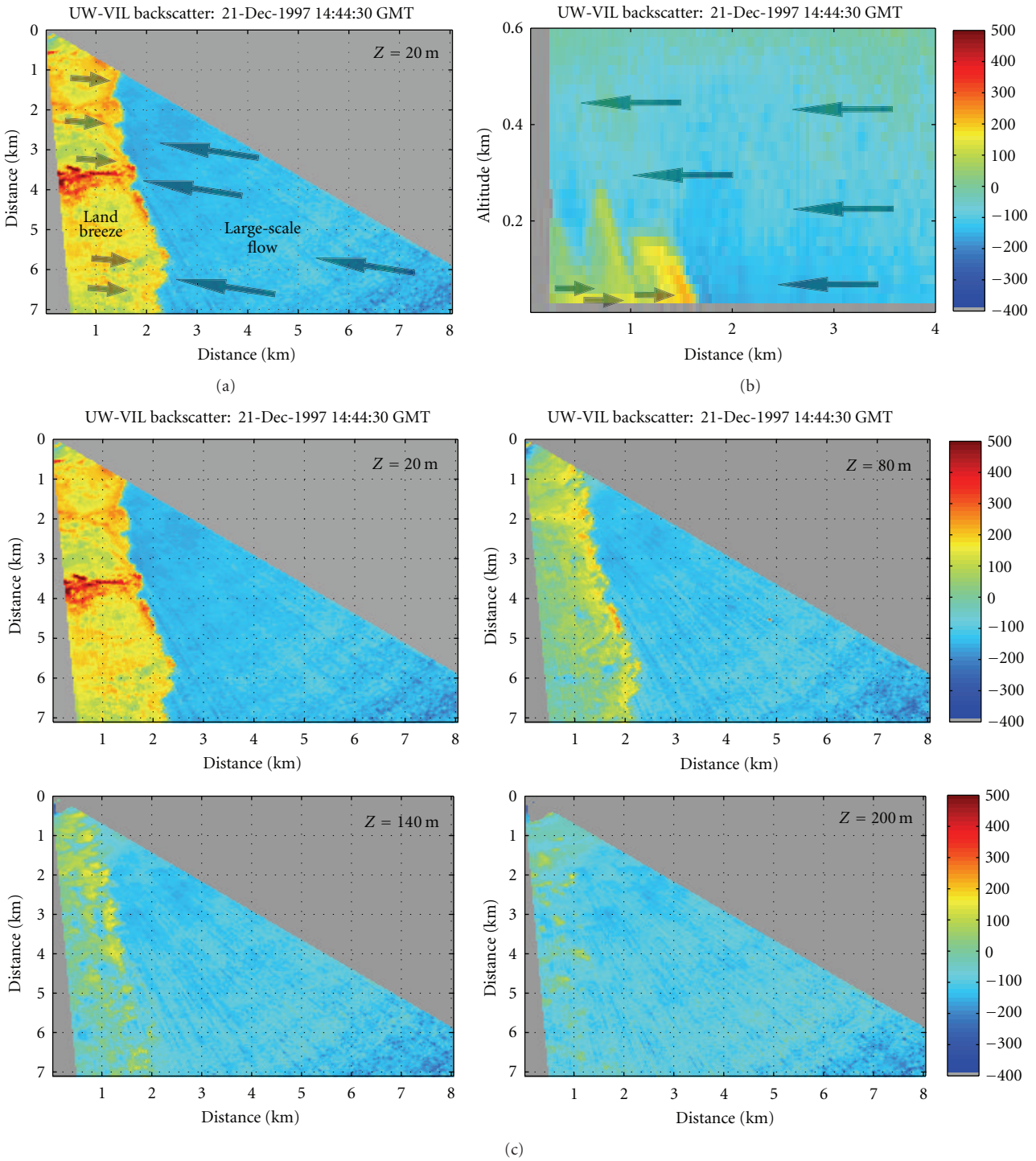

Figure 3: VIL scans from December 21, 1997 showing the land breeze flowing offshore. (a) shows a horizontal scan that captures the land breeze extending offshore. (b) is a vertical cross-section, showing the shallow land breeze extending offshore. (c) shows horizontal cross-sections at several elevations, illustrating the depth of the land breeze.

(PPI) in which the elevation angle is held constant, while the azimuthal angle is changed. Constant altitude PPIs (CAPPIs) are created through interpolation in an attempt to negate the angle at which the beam exits the transmitter relative to the earth's surface.

4. December 21 1997

The early morning of December 21 featured a surface anticyclone moving across the eastern Great Lakes into southeastern Canada (Figure 2). Surface winds at Sheboygan shifted

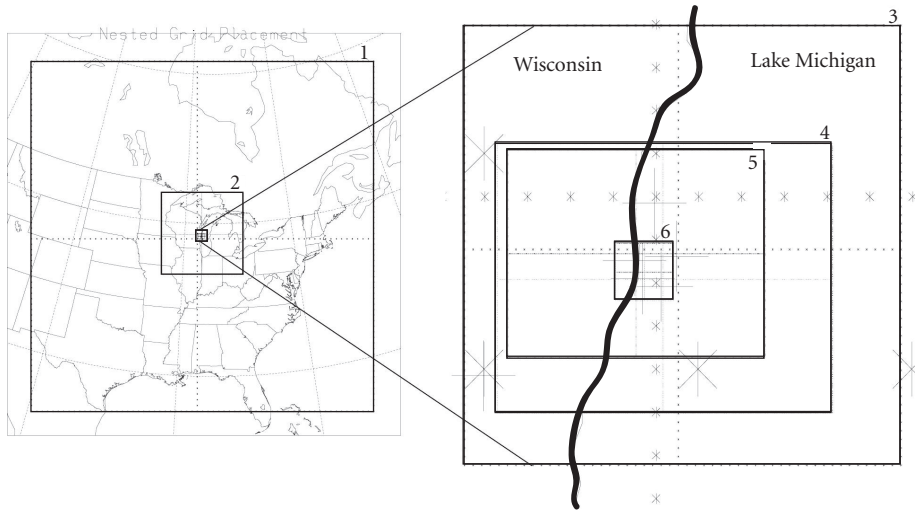

Grid number	Horizontal Points	Vertical Points	Horizontal Resolution (m)	Horizontal Size (km)	Vertical Resolution
1	65×65	50	60000	3780×3780	For ALL Grids: (i) 20 m resolution to 120 m above lake level (ii) Step increased by 120% to a maxstep of 750 m (iii) Uppermost level at 16.014 km
2	77×77	50	12000	900×900	
3	52×52	50	2400	120×120	
4	197×197	50	480	93.6×93.6	
5	452×362	50	160	72×57.6	
6	502×502	50	32	16×16	

Figure 4: The simulation grid-nesting scheme and grid properties.

from northwesterly to calm, and then to easterly. Synoptically forced winds were generally light, ranging from calm to 5-6 m s^{-1}. Surface temperatures ranged from -7°C during the early morning hours to near 0°C during the day, with prevailing winds advecting warmer air from over the Lake Michigan surface. Lake surface temperatures for the date were around 2.5–3°C.

Early VIL observations reveal a poorly defined land breeze extending approximately 9–10 km offshore. The land breeze can be seen in lidar data as a volume of increased backscatter extending offshore from the lidar site. There are two main reasons for increased backscatter within the land breeze. The first is that flow advecting offshore has a higher concentration of aerosol particles because of activity in the city of Sheboygan and at industrial sites upwind. Dust and other pollutants make the air relatively dirty when compared to air coming across the lake. Additionally, the land breeze has a higher relative humidity than air flowing across the lake in part due to its colder temperatures. Aerosols tend to swell in regions of high relative humidity [29–31], increasing their backscatter cross-sectional area.

As the easterly synoptic flow increases in strength, the land breeze is forced to retreat toward the shoreline. Figure 3 shows lidar imagery from 14:44 GMT. At this time the land breeze is well defined, extending only 1.5–2 km offshore (Figure 3(a)), and is much shallower with a vertical extent of only 100–200 m or so (Figure 3(b)). The nose of the land breeze shows up clearly at this point as a raised area formed along the most easterly point of the circulation, where it intersects with synoptic flow. Figure 3(c) shows horizontal cross-sections at different elevations. These reveal the shallow nature of the land breeze, with very little remaining at an altitude of only 140 m above lake level.

Eventually, a mesoscale front passed through and overpowered the land breeze. During this time, scientists at the lidar site recorded an increase in surface roughness of water approaching the shoreline, caused by stronger winds outside the land breeze, and winds over the shoreline shifted from a westerly land breeze to south-southeasterly.

5. Land Breeze Simulation

5.1. Simulation Configuration. Figure 4 reveals grid positioning and characteristics for the 6 grids implemented in this UW-NMS simulation. The outermost grid features 60-kilometer resolution and covers an area of 3780 km^2. The innermost domain features 32-meter resolution and covers only 16 km^2, positioned over the shoreline.

All domains share the same stretched vertical resolution. The first 15 levels are spaced at 20 m intervals, above which the grid is stretched by 120% to a maximum step size of 750 meters. The remaining levels are all 750 meters, resulting in the top of the simulation being positioned around 16 km above sea level. Since lake level at Sheboygan Point is

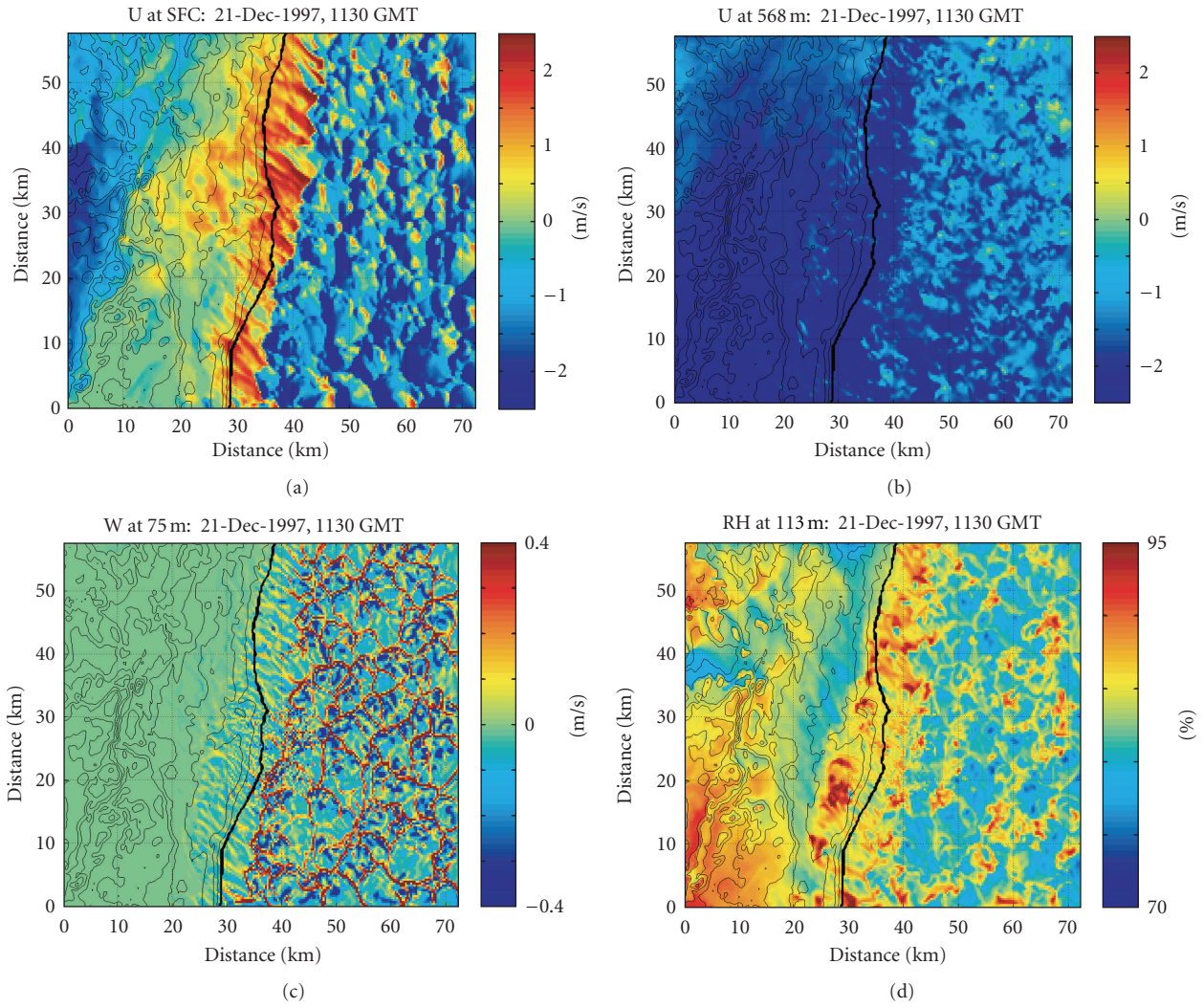

Figure 5: Simulation output from grid 5. The land breeze shows up very clearly in the surface zonal velocity field (a) and the return flow in the zonal velocity field at 570 m above lake level (b). The land breeze front and convective boundary layer is shown in the vertical velocity field at 75 m above lake level (c). The 113 m relative humidity field also shows very clearly the horizontal extent of the land breeze (d).

approximately 177 meters above sea level, and the maximum topographical elevations in the sixth domain are around 200 meters above sea level, approximately the lowest 100 meters above ground are at 20-meter vertical resolution.

The simulation is initialized using the ECMWF 00:00 GMT analysis from December 21. Additionally, a 100 m resolution topographical data set of the state of Wisconsin is utilized to most accurately represent the influence of these features on the flow.

5.2. Virtual Scattering. One element added to the simulations in order to better visualize the land breeze and complete comparison with lidar data is a virtual scattering parameter. With one major exception, the technique used follows that implemented in previous validation efforts of Lake-ICE LES simulations [32].

In an attempt to include the humidity effect on aerosol size in numerical simulation, previous works [32–34] had utilized a historical data set [31]. Here, in order to more accurately reproduce the characteristics of the studied aerosol population, the enhancement parameter is calculated directly from lidar data (see the Appendix). Use of the described technique led to the conclusion that the Fitzgerald data was not directly applicable to the current aerosol composition, and a new enhancement parameter was utilized. The data is well represented by the fit curve:

$$\alpha = 0.8 + \frac{80}{(100 - \mathrm{RH})^{1.98}}, \tag{1}$$

where RH is the relative humidity and α is the scattering coefficient. The aerosol is assumed to be dry at RH = 30% and the ratio of $\alpha(\mathrm{RH})$ to $\alpha(30)$ is used to determine swelling associated with that RH. This ratio is then multiplied by the model tracer concentration, and the log of that product is multiplied by a system constant to account for the log compression applied to the lidar data. Although exact values of backscatter will not match due to differences in aerosol concentration between the model and observed atmosphere,

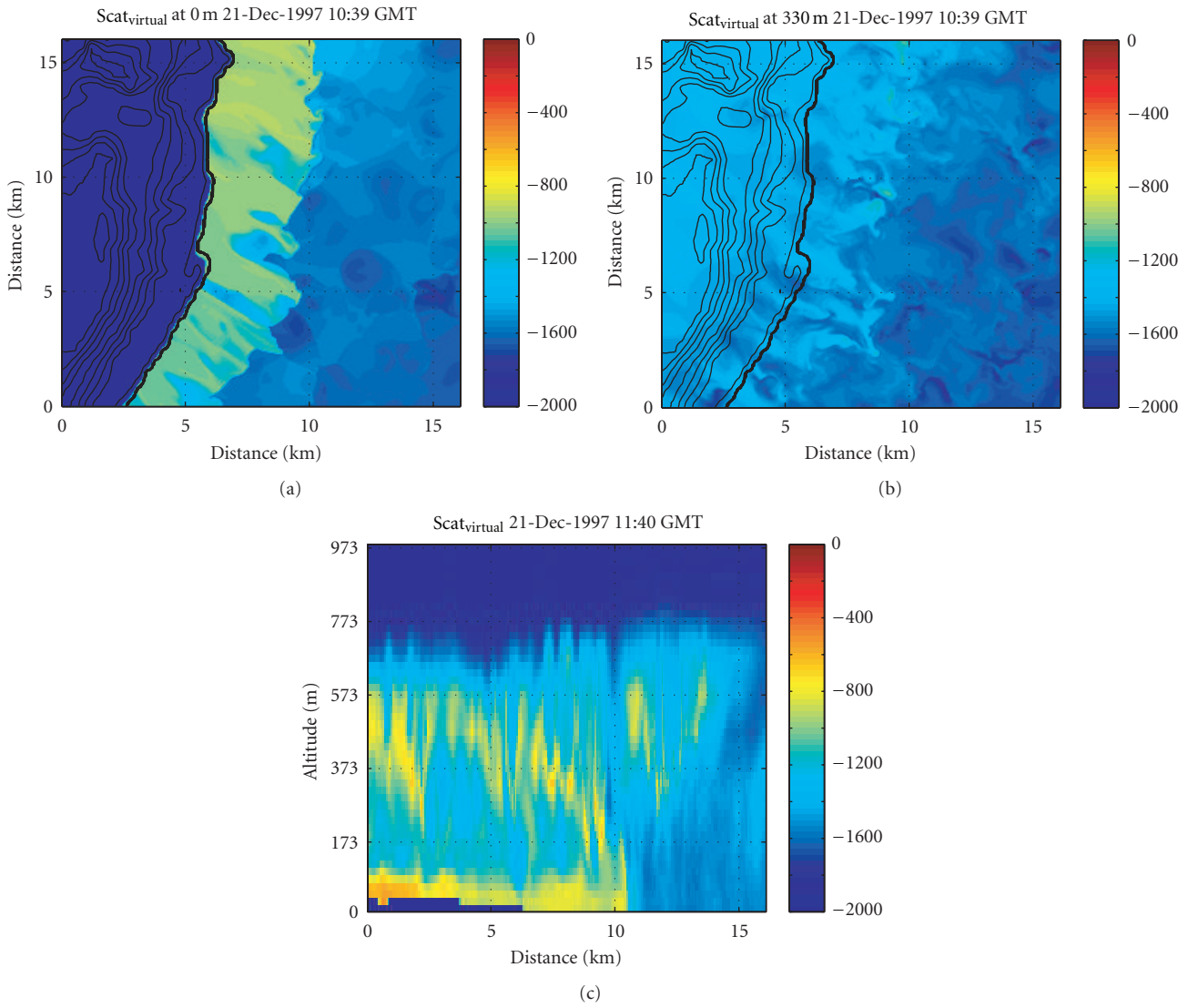

FIGURE 6: The simulated backscatter for grid 6. The land breeze at the surface is shown in (a) while (b) reveals a total lack of land breeze at 330 m above lake level. A vertical cross-section (c) reveals the shallow land breeze flowing offshore, as well as the boundary layer depth and a region of strong mixing above the land breeze.

the relative intensity of backscatter patterns within the individual data sets are what are important.

5.3. Simulation Results. Starting with the inner grid, it is very clear that the land breeze develops in the simulated atmosphere. Figure 5 shows results from the fifth domain, which was large enough to encompass the entire land breeze circulation. The zonal velocity plot reveals a very clear acceleration of flow at the surface (Figure 5(a)) from 5 to 10 km inland to around 5 km offshore. The intensity of the land breeze is relatively light (~0–3 m s^{-1}), with the strongest portions occurring over the lake. Offshore, the convective boundary layer shows up nicely, with winds generally being onshore at 1–4 m s^{-1}. Some variation in the zonal flow associated with convective eddies in this flow can be seen. At around 575 meters above lake level (Figure 5(b)), the return flow of the land breeze circulation is quite striking, with a pronounced westward acceleration of flow at the land breeze front and a stronger westward flow to around 20 km inland.

Figure 5(c) shows vertical velocity at 70 m above lake level. The offshore convective boundary layer is very noticeable here as cellular structures of stronger vertical velocity. Also notable is how individual cells penetrate westward into the land breeze deforming the frontal boundary between the land breeze and convective flow. At this intersection there is a convergence of flows along with an associated increase in upward motion. There is some variation in the strength of this frontal vertical motion, with sections that are perpendicular to the west-northwest flow of the land breeze having the strongest vertical velocities. Those sections of the boundary that are deformed by convective cells so that they are no longer perpendicular to the land breeze have weaker upward

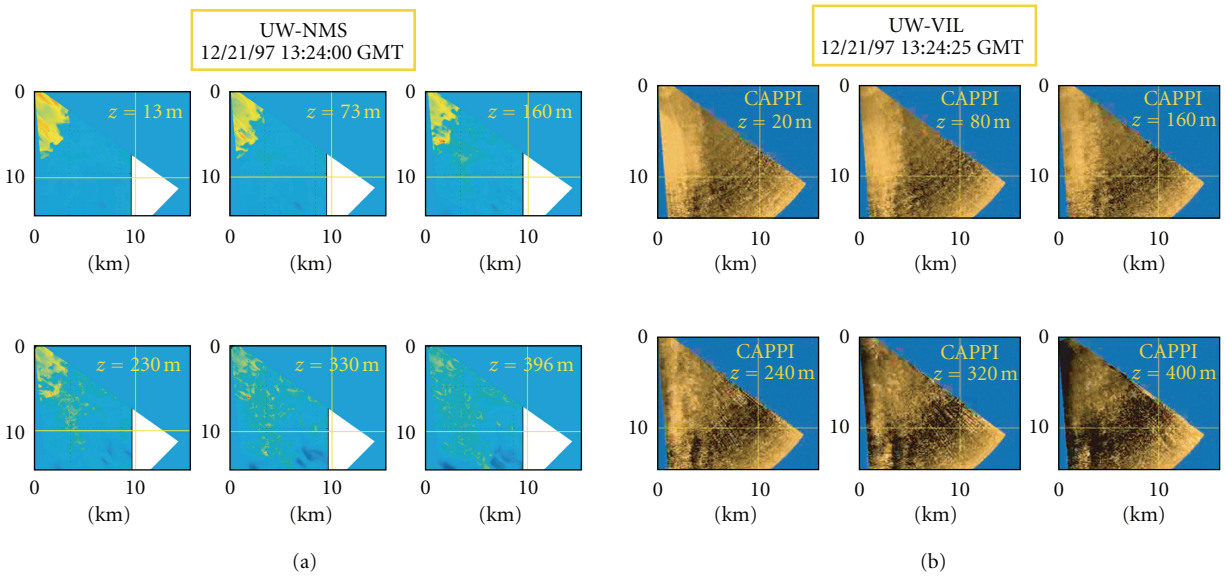

Figure 7: A comparison of the horizontal components of a virtual RHI-volume scan derived from the simulation virtual backscatter (a) and a VIL-produced RHI volume scan (b).

motion. There is little vertical motion within the land breeze itself.

Figure 5(d) shows the model relative humidity field at 113 meters above lake level. Due to a difference in temperature, the relative humidity of the land breeze is higher than that of the prevailing flow. Again, this fact aids in the detection of the circulation with the lidar, since aerosols will swell in higher relative humidity, leading to increased backscatter.

Examination of model scattering output reveals a clear land breeze extending to around 4 km offshore. This position is held near steady state until a mesoscale feature overpowers the circulation. A horizontal cross-section (Figures 6(a) and 6(b)) from the sixth domain shows that there are clear undulations in the land breeze front, and examination of several time steps reveals that this undulation represents a continual interaction between the land breeze and the convective prevailing flow coming across the lake. The vertical extent of the land breeze can be determined by looking at cross-sections from several elevations. Figure 6(a) is the surface simulated scatter. Figure 6(b) represents simulated backscatter at the same time at approximately 330 m above lake level. At this elevation the land breeze is already poorly defined with only the land breeze head, formed at the frontal region between the land breeze and prevailing flow, still showing any significant increase in scattering. Also noticeable in these figures is an apparent shoreline effect on the horizontal extent of the land breeze.

Additional analysis into the depth of the circulation can be completed utilizing a vertical cross-section of the scattering parameter (Figure 6(c)). The land breeze can be seen as a region of increased virtual scattering extending approximately 4 km offshore. The shoreline is located at approximately 6.5 km in this particular figure. This cross-section is from the 32 m resolution sixth domain. Of note here are the undulating nature of the top of the land breeze likely resulting from the wind shear at this location, the raised land breeze head at around 170 m above lake level, and the mixing that is going on over the land breeze. The sharp gradient at 650 to 800 m above lake level is the top of the boundary layer.

6. Simulation Validation

6.1. Spatial Accuracy of Land Breeze Simulation. To determine the ability of the UW-NMS to replicate the land breeze circulation, we utilize data from the UW-VIL. As mentioned earlier, the VIL data has the high temporal and spatial resolution required to complete a thorough and valid evaluation of the model's performance. Quantitative comparison between simulation output and lidar data is obtained via replication of lidar measurements in the simulation. Here, a preliminary effort has been made using the virtual scattering parameter introduced in Section 4 and the appendix.

A comparison of a model- and lidar-derived CAPPI scans from 13:24 GMT are shown in Figure 7. Qualitative analysis of this comparison reveals similar features in the appearance of simulated and observed land breezes. Both show the land breeze extending approximately 4 km offshore at lower altitudes. Also, there is striking similarity in the depths of the observed and simulated land breezes, with the land breeze more or less not affecting the aerosol field above 230 m above lake level. One distinct difference between the observed flow and the simulated one is that in the simulation (left) the offshore extent of the land breeze follows the shoreline more closely than in the observed flow. Although there is some curvature to the observed land breeze in the southern portion of the domain, mimicking the similar curve found in the shoreline at that location, it is far more pronounced in the simulation.

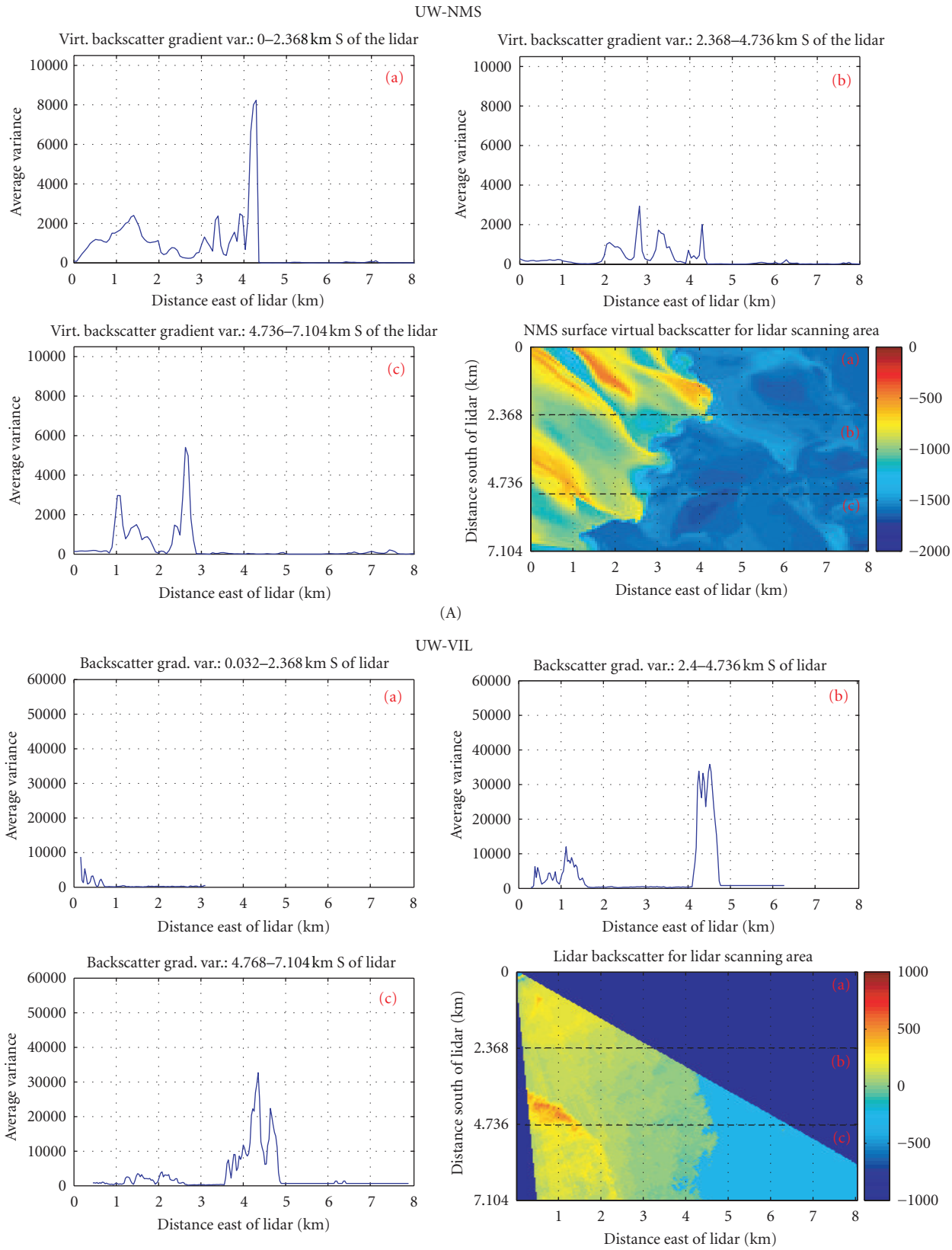

FIGURE 8: Backscatter gradient variance plots for the simulated backscatter (A) and lidar backscatter (B). Each of the three (a–c) regions represent horizontal average variances for the corresponding regions labeled (a–c) on the horizontal backscatter plots in the bottom right.

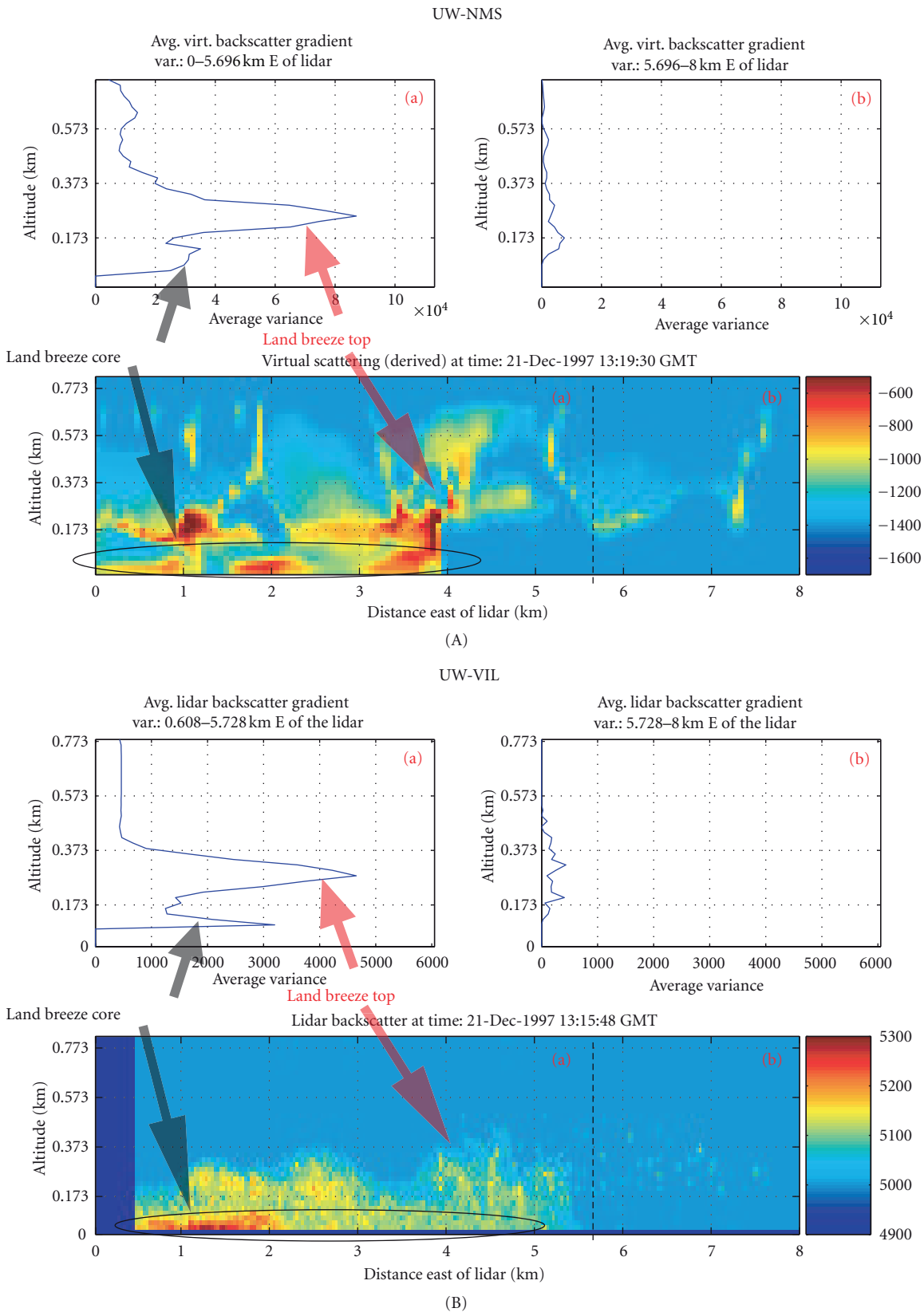

Figure 9: Backscatter gradient variance plots for the simulated backscatter (A) and lidar backscatter (B). Each of the two (a, b) regions represents vertical average variances for the corresponding regions labeled (a) and (b) on the vertical backscatter cross-sections underneath them. Marked in the variance plots are the depths of the land breeze and land breeze head.

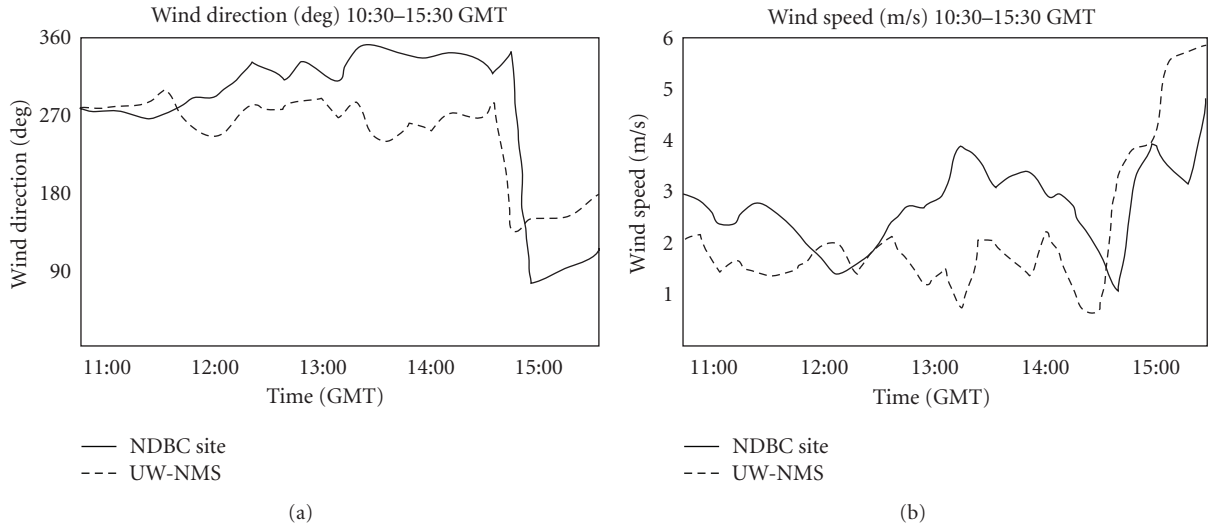

Figure 10: Wind direction (a) and speed (b) as measured at the NDBC site and as seen in the NMS simulation.

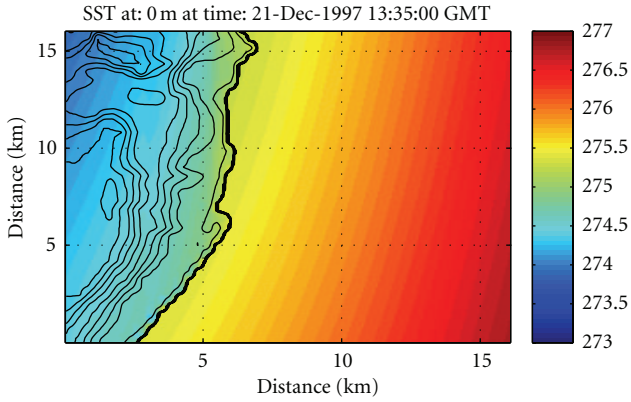

Figure 11: The model skin surface temperature. Note the horizontal extent of the gradient over the lake.

Calculating the variance of the scattering gradient results in additional analysis of virtual and observed backscatter. Figures 8 and 9 show this comparison for horizontal and vertical cross-sections, respectively. Here, the gradient variance (X) is calculated as follows:

$$X = \frac{1}{y_2 - y_1}\left(\sum_{y_1}^{y_2}\left(\overline{\Delta} - \Delta_x\right)^2\right), \tag{2}$$

where y_1 and y_2 are the bounds of the area over which the variance is averaged (not necessarily in the meridional direction), $\overline{\Delta}$ is the mean scattering gradient between two specific points over the area bounded by y_1, y_2 and the established extremes in the second dimension, and Δ_x represents the gradient between two specific points. In these examples, the gradient was calculated over 7 points in order to remove some of the higher-resolution noise from the calculation. Additionally, a low pass filter was applied to both the lidar data and the model output in order to remove any small gradients not relevant to the land breeze.

This calculation allows for the determination of land breeze front position in the horizontal case; in the vertical case, it allows for the determination of circulation depth and depth of the land breeze front. Additionally, looking at the east-west gradient in the horizontal cross-section, it is somewhat revealing of the meridional variance of the frontal position. A steady north-south horizontal front has a very well-defined peak, and sections of the front having any zonal orientation exhibiting a broader variance peak. It is again important to note that calculated variance values are not expected to match, since the virtual scattering parameter utilizes no data on exact aerosol concentrations. This is not a problem, as the relative concentration of aerosol from one position to the next will determine the backscatter gradient.

Looking at horizontal characteristics (Figure 8), it can be noted that around 13:00 GMT, observations show the land breeze extending slightly farther offshore than in the simulation. The simulated land breeze extends to around 4 km offshore, while the observed land breeze extends closer to 5 km offshore. Although both simulated and observed land breezes have associated undulating fronts, the simulated version appears to have more variation in position and orientation of the frontal zone, as can be seen by the broader variance peaks. Additionally, there is a larger variation of scattering intensity in the simulation across the frontal gradient, resulting in less well-defined peaks, particularly in the central analysis region (b). Another feature of note in the observed lidar backscatter is a strong gradient originating on the far western section of the center analysis region (b). This plume of increased backscatter is due to the additional aerosols injected into the atmosphere at an industrial region on the shoreline at this location and was regularly observed in the Lake-ICE observations.

Similar calculations were completed for vertical cross-sections (Figure 9). In these plots, the calculation was broken up over the western portion of the domain (containing the land breeze) and the eastern portion (outside the land

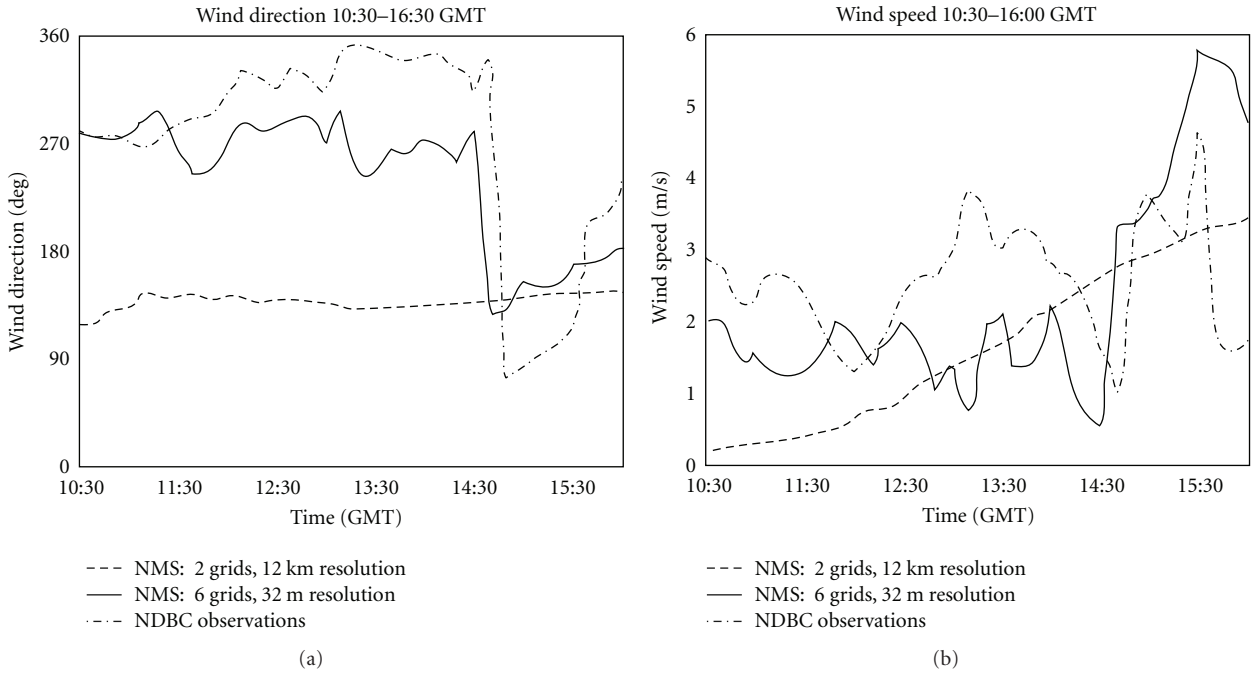

Figure 12: Wind direction (a) and speed (b) time series from the NDBC observations (dash-dot line), the 32 m NMS simulation (solid line) and the 12 km NMS simulation (dashed line).

breeze). Two distinct features can be extracted from the variance calculations here. First, there is the depth of the "core" of the land breeze extending out over the lake, shown at around 100 m in the simulation and the lidar data. The second feature is the depth of the top of the land breeze circulation. Both the simulation and lidar data show significant variation in this depth horizontally, with both fluctuating between 200 and 400 m above lake level. Variation in height is shown by the broader nature of the variance peak when compared to the core peak, particularly in the lidar observations.

Comparison of the measured and simulated wind speed and direction within the land breeze support the observed land breeze extending farther offshore than the simulated one. Although the wind direction (Figure 10(a)) in the simulated flow is more westerly, the speed (~1-2 m/s, Figure 10(b)) is only about half of that observed (~2–4 m/s). This significant difference in velocity would help to explain the discrepancy in the position of the land breeze front.

A central question in our evaluation of dynamical downscaling performance in this scenario revolves around the slight horizontal displacement of the simulated land breeze front. As noted above, the simulated land breeze was slightly weaker than that observed at the shoreline. Figure 11 shows the simulated skin surface temperature at the time of comparison. In the simulation, the near surface air temperature (not shown) over the shoreline ranged from −2° to 0°C, while the lake surface temperature ranges from 2° to 3.5°C. When compared to the observed values of −7° to 0°C and 2.5° to 3°C, respectively, this leads to a smaller temperature gradient. Additionally, the simulated gradient exists over 10–15 km horizontally, while the observed gradient was measured at the shoreline, over only a few hundred meters. A previously derived index to predict the likelihood of a lake breeze occurrence [35]:

$$\sigma = \frac{V_g^2}{C_p \Delta T} \tag{3}$$

includes V_g as the mean geostrophic wind speed, C_p as the specific heat of dry air, and ΔT as the difference between the maximum air temperature and mean water temperature over a given distance. A lower index value was shown to be related to conditions favorable to lake breeze development. In this example, assuming that V_g and C_p are constant, decreasing ΔT either through a decrease in the actual temperature difference, or a broadening of the distance over which this difference occurs, would increase sigma, resulting in a weaker or nonexistent land breeze.

6.2. Simulation Timing. In investigating the ability of the dynamical downscaling technique to recreate the general characteristics of the land breeze, an attempt was made to validate the ability of the technique to capture the timing and evolution of the event. In addition to accurate simulation of land breeze extent and intensity, the correct simulation of the timing of the demise of the land breeze circulation is equally important. In this particular situation, a mesoscale feature overpowered the land breeze and pushed it back over the shoreline and out of view of the lidar.

To test the downscaling technique's ability to replicate this termination of flow, simulated surface wind speed and direction are compared with those measured at the NDBC site located within 1 km of the lidar position. Figure 10 shows these comparisons for the lidar observation period.

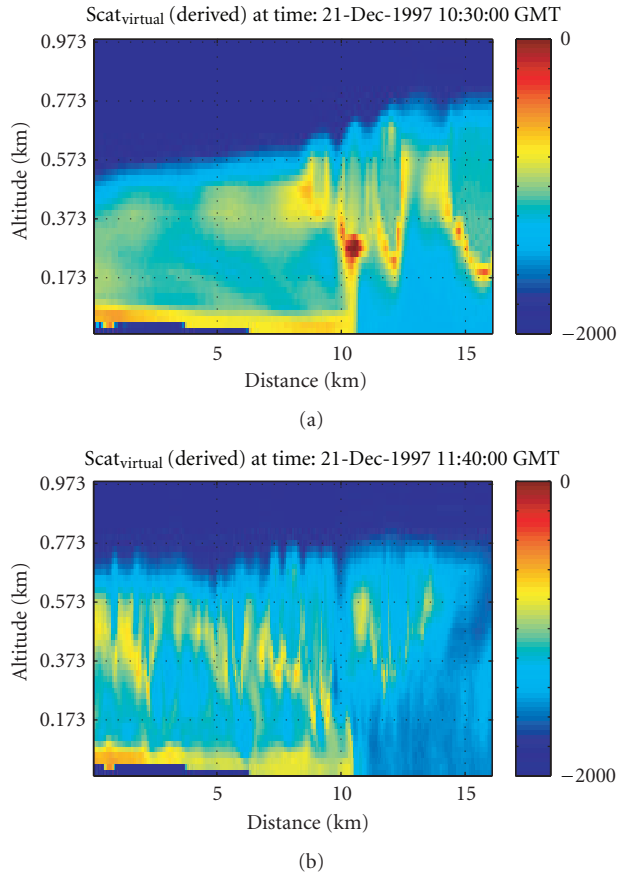

FIGURE 13: Vertical cross-sections of virtual backscatter from the fifth grid (a) and the sixth grid (b). Note the increased structure of the land breeze, as well as boundary layer, and the reduced depth of the land breeze head in the higher resolution cross-section.

Evaluation of wind direction (Figure 10(a)) for the time period shows strong agreement between simulation and observations. The point of interest in this comparison is the major shift in direction that takes place between 14:30 and 14:45 GMT. Winds shift from westerly/northwesterly to southeasterly/easterly. This reversal of wind direction marks the retreat of the land breeze front over the observation point. Comparison of simulated and observed wind speeds (Figure 10(b)) shows a corresponding increase at around 14:45 GMT, with winds strengthening from 1–3 m s^{-1} to 5-6 m s^{-1}.

6.3. Effect of Resolution. As mentioned in the introduction, an important outcome of this study is the determination of what benefits are gained by using very high-resolution domains. If a simple interpolation of a large-scale forecast leads to a similar solution to that attained in this study, then the use of the additional computational resources is not justified. To consider this issue, a comparison was done between the NDBC data, a typical "mesoscale" simulation (12 km horizontal resolution) using the UW-NMS with one nested grid, and the 6-grid UW-NMS simulation discussed above. Time series of wind speed and direction from these three sources are shown in Figure 12. It becomes obvious from the calculated wind direction (Figure 12(a)) that the 12 km simulation does not have sufficient resolution to portray the land breeze, as the winds are southeasterly the entire period. The wind speed comparison (Figure 12(b)) does show an increase toward the end of the period as is seen in the high-resolution simulation but without a corresponding change in wind direction, this demonstrates only the increase in the prevailing winds that eventually led to the collapse of the land breeze, not the presence of the land breeze itself.

Although the 12 km resolution is not sufficient in this case, the 160 m resolution of the 5th grid in the 6-grid simulation is. Here, the resolution utilized becomes justified by what is sought. If the position of the front is all that is needed, then the highest resolution grid is not necessary. A comparison of data from the 5th and 6th domains (Figure 13) shows that the increased resolution of the 6th grid allows for replication of more details in the simulated land breeze structure as well as in the boundary layer structure, most specifically in the form of the structure of the land breeze head and top boundary of the land breeze itself. Again, this suggests that there is more information to be gained through the utilization of higher resolution, but the need for that information should be evaluated on a case-by-case basis.

Additionally, here we must consider the difference between simulation spatial resolution and the resolution of the information used for initialization. In this example, although the simulation is run at 32 m resolution across the shoreline in the highest-resolution domain, and although the topographical dataset used features 100 m resolution, adequate for representation of an accurate shoreline, the land-lake temperature gradient appears to be smoothed by a lack of resolution in the skin surface temperature dataset used. This reduction in spatial information appears to lead to a weaker land breeze than that observed.

7. Discussion and Conclusions

The land breeze observed off Sheboygan Point, Wisconsin, on December 21 1997 was simulated using the University of Wisconsin Nonhydrostatic Modeling System. To validate the accuracy of the simulation, data collected using the University of Wisconsin Volume Imaging Lidar was utilized. Comparison of simulation scattering and lidar-observed backscatter reveals the ability of the model to replicate this microscale phenomenon. The simulated land breeze depth matches observations very closely. The horizontal position of the land breeze front does differ slightly between simulation and observations. It is believed that this difference is primarily caused by a difference in the observed and simulated lake and land surface and air temperatures.

The displacement of the land breeze front by small errors in surface qualities demonstrates a challenging issue in using dynamical downscaling as a valid technique for simulation of the atmospheric boundary layer. In the end, the simulation will still only be as good as the initial conditions that

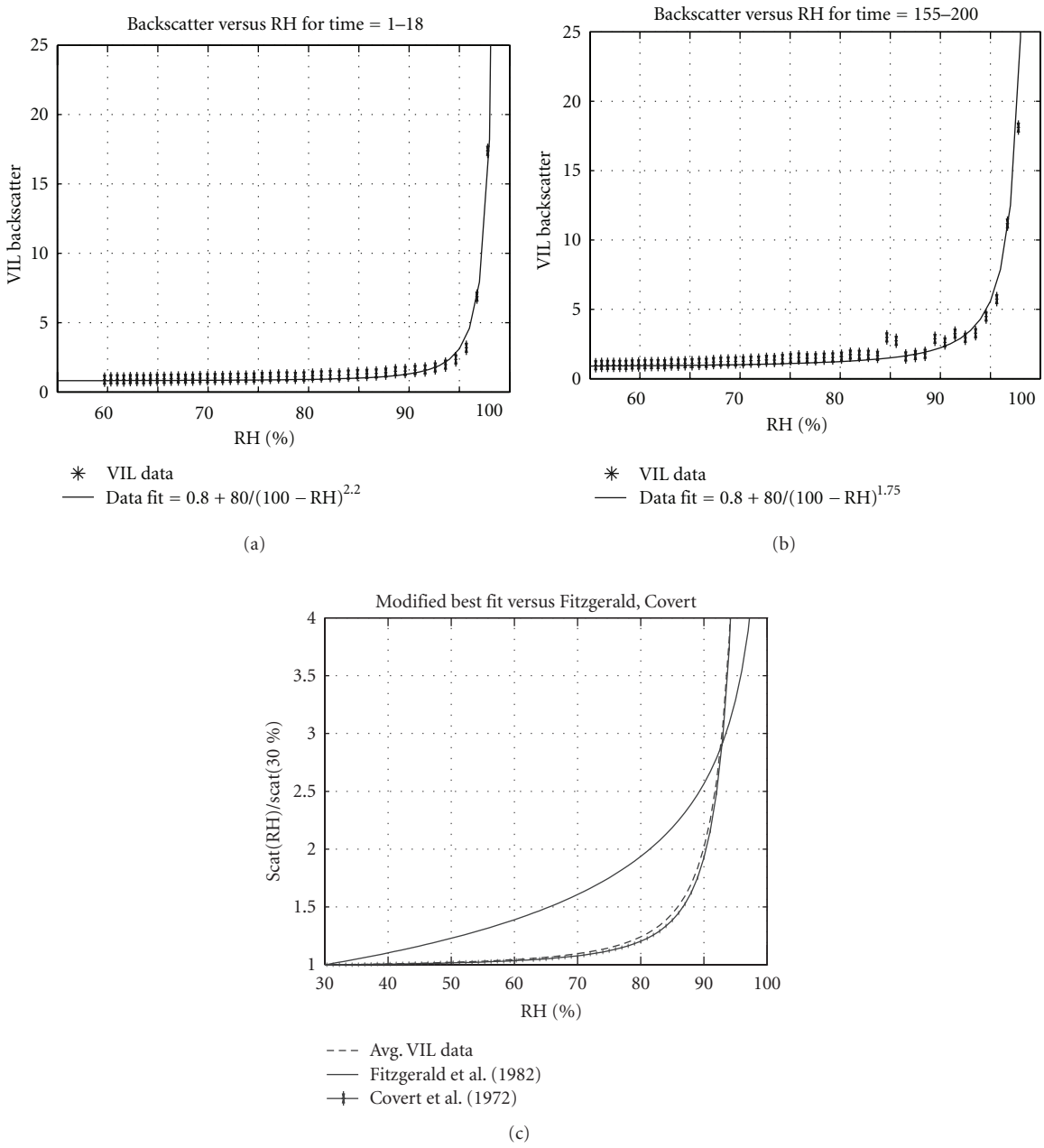

Figure 14: The ratio of backscatter at a relative humidity and the dry (RH = 30%) value as a function of relative humidity. (a) and (b) show VIL data from December 21, with a representative fit curve. (c) shows the average fit curve from the VIL data as compared to datasets collected by Fitzgerald and Covert.

are provided. In the case of the land breeze, not only are the quantities important, but the spatial resolution of the thermal gradient is as well. Perturbation of the boundary conditions around the "real" initial conditions may help with this issue, though it is likely that a spread of solutions would be produced that simply encompasses the current error. Additionally, running ensembles at these resolutions would require a huge amount of computer power, and makes this solution impractical for long integration times, large domains, or real-time forecasting. Therefore, continued improvement of the initialization data sets at high resolutions is likely very important to the success of dynamically downscaled simulations.

Despite the shortcomings discussed above, results show accurate simulation of structural components of the land breeze circulation, as well as the timing of the decay of the simulated circulation. Decay was primarily the result of a large-scale wind shift, an event that would not have been simulated using traditional LES. The high accuracy of simulation timing in this case illustrates that the predictability of

specific boundary layer flows and certain microscale features therein is likely strongly linked to the predictability of large-scale flow. This observation leads to the conclusion that continued improvement of large-scale modeling, measurements, and assimilation could have substantial impact on high-resolution forecasting at the microscale and that the correct incorporation of the large-scale evolution is of vital importance to correct simulation at the small scale.

Appendix

Calculation of Relevant Backscatter versus Relative Humidity Profile from VIL Data. In order to more closely simulate scattering in the simulation output, a virtual scattering technique was implemented. This technique utilizes a model passive tracer along with the model relative humidity profile. In order to introduce an aerosol population into the simulated domain, the passive tracer is initialized at the lowest two above-surface grid points at model start time. This tracer is then allowed to advect throughout the entire model domain. There are no additional sources or sinks, so the tracer concentrations are simply the result of atmospheric mixing and divergence.

In addition to the passive tracer concentrations, data from the simulation relative humidity field is used to reproduce the effect of relative humidity on aerosol concentration. For this particular study, rather than utilizing previous measurements of the humidity effect, a curve representing this effect was extracted directly from the lidar data.

In order to extract the needed data, it was assumed that the region offshore from the land breeze front was a well-mixed boundary layer with an adiabatic temperature profile. In addition, it was assumed that the relative humidity at cloud base, as seen by a sharp increase in lidar backscatter, is equal to 100%. These two assumptions along with knowledge of the surface temperature allow us to calculate a relative humidity profile for the subcloud layer. This profile can be compared with the backscatter profile for the same layer to determine a backscatter-RH relationship. Figure 14(a) shows a plot of the derived backscatter-RH profile for 18 seconds of scanning data, along with a fit curve to this data. Figure 14(b) shows a similar plot for a 45-second period, and the fit curve to that data. Figure 14(c) shows the ratio of the value of the backscatter-RH relationship at a relative humidity to its value at RH = 30% for an average VIL profile, the Fitzgerald derived profile from Washington D.C. used in previous studies, and a dataset measured by Covert in Denver, Colorado in 1972. Here, it becomes obvious that the Fitzgerald data set is not representative of the aerosol population found over Lake Michigan on the date in question.

Acknowledgments

The authors wish to acknowledge support from the US National Science Foundation during the completion of this paper. Additionally, the authors would like to thank the numerous people involved with the collection of data during Lake-ICE. Finally, the authors would like to thank the editorial board of the journal for the constructive comments made to help improve this paper.

References

[1] J. C. Wyngaard, L. J. Peltier, and S. Khanna, "LES in the surface layer: surface fluxes, scaling, and SGS modeling," *Journal of the Atmospheric Sciences*, vol. 55, no. 10, pp. 1733–1754, 1998.

[2] C. H. Moeng and P. P. Sullivan, "A comparison of shear- and buoyancy-driven planetary boundary layer flows," *Journal of the Atmospheric Sciences*, vol. 51, no. 7, pp. 999–1022, 1994.

[3] I. Orlanski, "A rational subdivision of scales for atmospheric processes," *Bulletin of the American Meteorological Society*, vol. 56, pp. 527–530, 1975.

[4] B. W. Atkinson, *Meso-Scale Atmospheric Circulations*, Academic Press, New York, NY, USA, 1981.

[5] G. J. Tripoli, "Numerical study of the 10 January 1998 lake-effect bands observed during Lake-ICE," *Journal of the Atmospheric Sciences*, vol. 62, no. 9, pp. 3232–3249, 2005.

[6] P. B. Duffy, R. W. Arritt, J. Coquard et al., "Simulations of present and future climates in the Western United States with four nested regional climate models," *Journal of Climate*, vol. 19, no. 6, pp. 873–895, 2006.

[7] L. Sun, D. F. Moncunill, H. Li, A. D. Moura, and F. A. S. Filho, "Climate downscaling over Nordeste, Brazil, using the NCEP RSM97," *Journal of Climate*, vol. 18, no. 4, pp. 551–567, 2005.

[8] Y. Liu, D. L. Zhang, and M. K. Yau, "A multiscale numerical study of Hurricane Andrew (1992). Part I: explicit simulation and verification," *Monthly Weather Review*, vol. 125, no. 12, pp. 3073–3093, 1997.

[9] Y. Jin, W. T. Thompson, S. Wang, and C. S. Liou, "A numerical study of the effect of dissipative heating on tropical cyclone intensity," *Weather and Forecasting*, vol. 22, no. 5, pp. 950–966, 2007.

[10] D. L. Zhang and J. M. Fritsch, "Numerical simulation of the meso-B scale structure and evolution of the 1977 Johnstown flood. Part I: model description and verification," *Journal of the Atmospheric Sciences*, vol. 43, no. 18, pp. 1913–1943, 1986.

[11] C. L. Ziegler, T. J. Lee, and R. A. Pielke, "Convective initiation at the dryline: a modeling study," *Monthly Weather Review*, vol. 125, no. 6, pp. 1001–1026, 1997.

[12] C. S. Keen, W. A. Lyons, and J. A. Schuh, "Air pollution transport studies in a coastal zone using kinematic diagnostic analysis," *Journal of Applied Meteorology*, vol. 18, no. 5, pp. 606–615, 1979.

[13] A. Clappier, A. Martilli, P. Grossi et al., "Effect of sea breeze on air pollution in the greater Athens area. Part I: numerical simulations and field observations," *Journal of Applied Meteorology*, vol. 39, no. 4, pp. 546–562, 2000.

[14] R. E. Passarelli and R. R. Braham, "The role of the winter land breeze in the formation of Great Lake snow storms," *Bulletin American Meteorological Society*, vol. 62, no. 4, pp. 482–491, 1981.

[15] R. J. Ballentine, "Numerical simulation of land-breeze-induced snowbands along the Western shore of Lake Michigan," *Monthly Weather Review*, vol. 110, no. 11, pp. 1544–1553, 1982.

[16] J. B. Elsner, J. R. Mecikalski, and A. A. Tsonis, "A shore-parallel cloud band over Lake Michigan," *Monthly Weather Review*, vol. 117, no. 12, pp. 2822–2823, 1989.

[17] M. R. Hjelmfelt, "Numerical study of the influence of environmental conditions on lake-effect snowstorms over Lake

Michigan," *Monthly Weather Review*, vol. 118, no. 1, pp. 138–149, 1990.

[18] M. R. Hjelmfelt, "Orographic effects in simulated lake-effect snowstorms over Lake Michigan," *Monthly Weather Review*, vol. 120, no. 2, pp. 373–377, 1992.

[19] H. Jeffreys, "On the dynamics of wind," *Quarterly Journal of the Royal Meteorological Society*, vol. 48, no. 201, pp. 29–48, 1922.

[20] B. Haurwitz, *Dynamic Meteorology*, McGraw-Hill, New York, NY, USA, 1941.

[21] B. Haurwitz, "Comments on the sea-breeze circulation," *Journal of Meteorology*, vol. 4, no. 1, pp. 1–8, 1947.

[22] F. H. Schmidt, "An elementary theory of the land- and sea-breeze circulation," *Journal of Meteorology*, vol. 4, no. 1, pp. 9–20, 1947.

[23] M. A. Estoque, "The sea breeze as a function of the prevailing synoptic situation," *Journal of the Atmospheric Sciences*, vol. 19, no. 3, pp. 244–250, 1962.

[24] Shiyuan Zhong and E. S. Takle, "The effects of large-scale winds on the sea-land-breeze circulations in an area of complex coastal heating," *Journal of Applied Meteorology*, vol. 32, no. 7, pp. 1181–1195, 1993.

[25] D. A. R. Kristovich, G. S. Young, J. Verlinde et al., "The lake-induced convection experiment and the snowband dynamics project," *Bulletin of the American Meteorological Society*, vol. 81, no. 3, pp. 519–542, 2000.

[26] N. A. Phillips and J. Shukla, "On the strategy of combining coarse and fine meshes in numerical weather prediction," *Journal of Applied Meteorology*, vol. 12, no. 5, pp. 763–770, 1973.

[27] T. L. Clark and R. D. Farley, "Severe downslope windstorm calculations in two and three spatial dimensions using anelastic interactive grid nesting: a possible mechanism for gustiness," *Journal of the Atmospheric Sciences*, vol. 41, no. 3, pp. 329–350, 1984.

[28] G. J. Tripoli, "A nonhydrostatic mesoscale model designed to simulate scale interaction," *Monthly Weather Review*, vol. 120, no. 7, pp. 1342–1359, 1992.

[29] D. S. Covert, R. J. Charlson, and N. C. Ahlquist, "A study of the relationship of chemical composition and humidity to light scattered by aerosols," *Journal of Applied Meteorology*, vol. 11, no. 6, pp. 968–976, 1972.

[30] J. W. Fitzgerald, W. A. Hoppel, and M. A. Vietti, "The size and scattering coefficient of urban aerosol particles at Washington, DC as a function of relative humidity," *Journal of the Atmospheric Sciences*, vol. 39, no. 8, pp. 1838–1852, 1982.

[31] D. E. Day and W. C. Malm, "Aerosol light scattering measurements as a function of relative humidity: a comparison between measurements made at three different sites," *Atmospheric Environment*, vol. 35, no. 30, pp. 5169–5176, 2001.

[32] S. D. Mayor, G. J. Tripoli, and E. W. Eloranta, "Evaluating large-eddy simulations using volume imaging lidar data," *Monthly Weather Review*, vol. 131, no. 7, pp. 1428–1452, 2003.

[33] S. D. Mayor, *Volume imaging lidar observations and large-eddy simulations of convective internal boundary layers [Ph.D. thesis]*, The University of Wisconsin—Madison, Madison, Wis, USA, 2001.

[34] G. de Boer, *Nested high resolution simulation and lidar validation of a land breeze circulation [M.S. thesis]*, Department of Atmospheric and Oceanic Sciences, The University of Wisconsin—Madison, Madison, Wis, USA, 2004.

[35] W. A. Lyons, "The climatology and prediction of the Chicago Lake breeze," *Journal of Applied Meteorology*, vol. 11, no. 8, pp. 1259–1270, 1972.